



## RESEARCH ARTICLE

# Fluorine-19 Cellular MRI Detection of *In Vivo* Dendritic Cell Migration and Subsequent Induction of Tumor Antigen-Specific Immunotherapeutic Response

Corby Fink,<sup>1</sup> Michael Smith,<sup>1</sup> Jeffrey M. Gaudet,<sup>2</sup> Ashley Makela,<sup>2</sup> Paula J. Foster,<sup>2</sup> Gregory A. Dekaban<sup>1</sup>

<sup>1</sup>Molecular Medicine Research Laboratories, Robarts Research Institute and Department of Microbiology and Immunology, University of Western Ontario, 1151 Richmond Street North, London, Ontario, N6A 5B7, Canada

<sup>2</sup>Imaging Research Laboratories, Robarts Research Institute and Department of Medical Biophysics, University of Western Ontario, 1151 Richmond Street North, London, Ontario, N6A 5B7, Canada

### Abstract

**Purpose:** A major hurdle in the advancement of cell-based cancer immunotherapies is the inability to track *in vivo* therapeutic cell migration. With respect to dendritic cell (DC)-based cancer immunotherapies, this lack of knowledge represents an even greater hurdle as the quantity of tumor-antigen specific DC reaching a secondary lymphoid organ post injection is predictive of the magnitude of the ensuing tumor-specific immune response. We propose fluorine-19 (F-19) cellular magnetic resonance imaging (MRI) as a suitable and non-invasive imaging modality capable of detecting and quantifying DC migration *in vivo* and thus, serving as a surrogate marker of DC-based immunotherapeutic effectiveness.

**Procedures:** Murine DC were generated from bone marrow precursors and labeled with a [<sup>19</sup>F]perfluorocarbon ([<sup>19</sup>F]PFC)-based cell labeling agent. DC were characterized by viability and phenotyping assessments as well as characterized by ability to induce *in vivo* tumor-specific immune responses following immunization in a B16-F10 mouse model of melanoma. The *in vivo* migration of [<sup>19</sup>F]PFC (PFC)-labeled DC was first compared to control unlabeled DC by microscopy and then measured using F-19 cellular MRI.

**Results:** Culture conditions were optimized such that > 90 % of DC labeled with PFC without affecting viability, phenotype, and function. This optimization permitted consistent detection of PFC-labeled DC migration using F-19 cellular MRI and resulted in the first successful comparison of *in vivo* migration between PFC-labeled and control unlabeled therapeutic cells of the same origin. PFC-labeled DC are migration-competent *in vivo* in a B16-F10 tumor-bearing mouse model.

**Conclusions:** We report a non-invasive and longitudinal imaging modality capable of detecting and quantifying therapeutic cell migration at both 9.4 and 3 Tesla (T) and suitable for therapeutic cell tracking in a tumor-bearing mouse model. F-19 MRI cell tracking is broadly applicable across disease states and is conducive to clinical translation.

**Key words:** Dendritic cell (DC), Fluorine-19 (F-19), Cellular magnetic resonance imaging (MRI), Cancer immunotherapy

## Introduction

A pressing need for the development of novel strategies to combat cancer exists for patients who are non-responsive to standard of care treatment options or who progress to a metastatic state [1]. One such emerging strategy is cancer immunotherapy, which includes exploiting the professional antigen presenting cell (APC) ability of dendritic cells (DC) to elicit *de novo* tumor-associated antigen (TAA)-specific cell- and humoral-mediated adaptive immune responses. Additionally, DC contribute to the activation of innate immune cells like natural killer (NK) cells, NK T cells, and macrophages that further promote and enhance TAA-specific immune responses [2, 3].

DC must locate to secondary lymphoid organs like the lymph node to exert their function in the context of DC-based cancer immunotherapy [4]. In fact, the number of DC reaching a lymph node is predictive of the magnitude of the resulting TAA-specific immune response [5, 6]. Although associated with excellent safety profiles spanning a multitude of immunogenic cancers, the overall effectiveness is suboptimal as consistently 5 % or less of peripherally injected DC reach secondary lymphoid organs [7–10]. At present, the lack of a non-invasive imaging modality capable of tracking and quantifying *in vivo* DC migration hinders the development of improved DC-based immunotherapies that result in long-term progression-free survival.

We propose fluorine-19 (F-19) cellular magnetic resonance imaging (MRI) as a suitable imaging platform to monitor therapeutic cell migration *in vivo* [11, 12] that overcomes limitations associated with previously used imaging modalities. These include the lack of anatomical information and the short half-lives of radiotracers hindering longitudinal radionuclide-based imaging [13] as well as superparamagnetic iron oxide (SPIO)-based cellular MRI impeding *in vivo* migration and, at best, being semi-quantitative [14, 15]. Previously, research has demonstrated that therapeutic cells such as human and murine DC and human peripheral blood mononuclear cells (PBMC) were F-19 MRI-detectable *in vivo* via incorporation of a [<sup>19</sup>F]perfluorocarbon ([<sup>19</sup>F]PFC) cell labeling agent [16–18]. Thus, we focused on comparing the *in vivo* migration and subsequent induction of a TAA-specific CD8<sup>+</sup> cytotoxic T lymphocyte (CTL) response between [<sup>19</sup>F]PFC (PFC)-labeled and unlabeled bone marrow-derived DC (BMDC). Furthermore, we report for the first time detection and quantification of migrating PFC-labeled DC *in vivo* with F-19 MRI on a 3-Tesla (T) clinical MRI scanner.

## Materials and Methods

### Animals

C57BL/6 mice were purchased from Charles River Laboratories (Wilmington, USA). B6.Cg-Tg(CAG-

DsRed\*<sup>+</sup>MST) 1Nagy/J (DsRed<sup>+</sup>) mice originally from Jackson Laboratories (Bar Harbor, USA) were kindly provided by Dr. Steven Kerfoot (University of Western Ontario). All applicable institutional and/or national guidelines for the care and use of animals were followed.

### Murine BMDC Generation

Mature BMDC were prepared based on the method of Inaba et al. and Dekaban et al. [15, 19] with modifications provided in electronic supplementary material (ESM). Bone marrow progenitor cells were cultured for 4 days in complete RPMI media containing granulocyte-macrophage colony-stimulating factor (GM-CSF) and interleukin (IL)-4 [15]. Day 4 immature BMDC were enriched by Histodenz<sup>TM</sup> gradient centrifugation. PFC (2.5–7.5 mg/ml, Celsense Inc., Pittsburgh, USA) was added to culture on day 4 post enrichment, with a previously described maturation cocktail added on day 5 of culture [20]. BMDC cultured without PFC served as control cells. On day 6 of culture, BMDC viability (Annexin V/7-Aminoactinomycin D (7-AAD)) and phenotype (CD11c, CCR7, CD86) were determined by flow cytometry and data acquired on a LSRII analytical flow cytometer (BD Biosciences, San Jose, USA).

### Adoptive Cell Transfer

BMDC were collected, washed in PBS, and formulated for subcutaneous hind footpad injections (in 40  $\mu$ l PBS) into C57BL/6 mice. In one experiment,  $1 \times 10^6$  or  $2.5 \times 10^6$  PFC-labeled BMDC injections were performed immediately following CellTrace<sup>TM</sup> CFSE (CFSE) incorporation, with the identical number of CFSE<sup>+</sup> control, unlabeled BMDC being injected into the contralateral footpad ( $n=7$  mice per condition). DsRed<sup>+</sup> BMDC adoptive cell transfer is available in ESM.

In a different experiment, four mice received a left and right popliteal lymph node pre-treatment of IL-1 $\beta$  (300 ng) 3 h prior to adoptive cell transfer and the remaining three mice did not receive pre-treatment. The hind footpads of these seven mice were injected with  $3 \times 10^6$  PFC-labeled BMDC. The last set of adoptive transfers included three injection conditions: control BMDC, SIINFEKL peptide-loaded control BMDC, and SIINFEKL peptide-loaded PFC-labeled BMDC. Peptide loading consisted of a 2-h incubation with SIINFEKL (0.2  $\mu$ g/ml). After loading,  $2.5 \times 10^6$  BMDC injections into both footpads for all three conditions were performed into tumor-naïve mice ( $n=5-7$  mice per condition) or  $3 \times 10^6$  BMDC footpad injections were adoptively transferred into B16-F10 tumor-bearing mice ( $n=4-5$  mice per condition).

### *MRI of BMDC Migration*

Where required, F-19 cellular MRI took place 48 h after footpad injection. A 9.4-T Varian small animal MRI scanner (Santa Clara, CA, USA) was used for tumor-naïve mouse imaging and a 3-T clinical MRI scanner (General Electric, ON, CA) was used for tumor-bearing mouse proton/F-19 imaging. A 3D-balanced steady state free precession (bSSFP) sequence and removal of F-19 isoflurane signal [12] was employed at both 9.4 and 3 T, with all parameters described in detail in ESM.

### *Popliteal Lymph Node Histology*

Mice that received CFSE<sup>+</sup> or DsRed<sup>+</sup> BMDC injections were euthanized 48 h after adoptive cell transfer and popliteal lymph nodes were removed. After cryopreservation in sucrose, 16 µm cryosections were prepared and imaged using an Olympus IX50 phase contrast inverted microscope (Richmond Hill, CA) and Infinity3-3URF camera (Lumenera, Ottawa, CA). Image Pro Plus 7.0 software (Media Cybernetics, Rockville, MD, USA) was utilized for morphometric analysis and represented as area of fluorescence/area of lymph node.

### *Quantification of In Vivo SIINFEKL-Specific Immune Response*

Mice that received  $2.5 \times 10^6$  control BMDC, SIINFEKL-presenting control BMDC, and SIINFEKL-presenting PFC-labeled BMDC were left for 7 days after injection, at which time mice were euthanized, popliteal lymph nodes removed, and a single cell suspension generated for each individual mouse. Flow cytometry was employed to identify CD3ε<sup>+</sup>CD8α<sup>+</sup> (CD3<sup>+</sup>CD8<sup>+</sup>) T cells and subsequent staining using a Class I iTAg MHC tetramer, H-2K<sup>b</sup>/PE SIINFEKL, identified SIINFEKL-specific CD8<sup>+</sup> T cells for each injection condition.

### *Statistical Analysis*

All data was presented as the mean ± standard error of the mean (SEM). A *t* test, one- and two-way ANOVA with Tukey's multiple comparison test, and Kaplan-Meier survival analysis (Graph Pad Prism, Version 7, La Jolla, USA) were used. Significance was considered if  $p \leq 0.05$ .

## **Results**

### *CD11c<sup>+</sup> BMDC Can Be Efficiently Labeled With PFC Without Affecting Viability or Phenotype*

Following 6 days in culture, > 80 % of cells were mature CD11c<sup>+</sup>CCR7<sup>+</sup>CD86<sup>+</sup> BMDC (Fig. 1a–c). Subsequently,

BMDC were stained with Annexin V/7-AAD to determine viability (Fig. 1d) in the presence of increasing concentrations of PFC, ranging from 2.5 to 7.5 mg/ml. Compared to control unlabeled BMDC, PFC labeling did not affect BMDC phenotype across the concentrations of PFC tested (Fig. 1e). BMDC viability was unaffected by PFC at concentrations of 2.5 mg/ml ( $89.43 \pm 0.77$  %) and 5.0 mg/ml ( $86.71 \pm 1.71$  %), yet significantly decreased at 7.5 mg/ml of PFC ( $77.36 \pm 5.17$  %; Fig. 1f). Increasing the PFC concentration from 2.5 to 5.0 mg/ml resulted in a 1.7-fold increase in the amount of fluorine incorporated per cell ( $1.783 \pm 0.141 \times 10^{12}$  F-19 spins/cell) and was not significantly increased at 7.5 mg/ml (Fig. 1g). Using a red fluorescent version of PFC (5 mg/ml), 92.3 % of BMDC incorporated PFC label compared to unlabeled BMDC (Fig. 1h). All subsequent labeling experiments were conducted with 5 mg/ml of PFC.

### *PFC Labeling of BMDC Does Not Impede In Vivo Migration*

A comparison of PFC-labeled BMDC and control BMDC migration was determined. BMDC were first confirmed to have the same phenotype as outlined in Fig. 1a–c and then, prior to injection, labeled with CFSE. Compared to an aliquot of BMDC removed before CFSE labeling (Fig. 2a/b, gray histograms), 100 % of PFC-labeled BMDC (Fig. 2a), and control, unlabeled BMDC (Fig. 2b) incorporated an equivalent amount of CFSE based on mean fluorescence intensity (MFI). Thus, CFSE fluorescence served as an accurate readout to compare *in vivo* migration between these two conditions.

*In vivo* migration to popliteal lymph nodes was assessed following low ( $1 \times 10^6$ ) and high ( $2.5 \times 10^6$ ) dose PFC-labeled BMDC hind footpad injection with equal numbers of CFSE<sup>+</sup> control BMDC administered in the contralateral footpad ( $N=2$ ; first trial,  $n=3$  per condition; second trial,  $n=4$  per condition). After 48 h, popliteal lymph nodes were removed to quantify fluorescence by digital morphometry. Representative images of CFSE<sup>+</sup> PFC-labeled BMDC and CFSE<sup>+</sup> control BMDC for both low and high injection doses appear in Fig. 2c/e and Fig. 2d/f, respectively. CFSE<sup>+</sup> BMDC were detected in central paracortical T cell-rich zones of the lymph node. As the digital morphometric data from two experiments was not different, the data was combined. Quantification of CFSE fluorescence demonstrated that PFC does not appear to impede BMDC *in vivo* migration compared to control BMDC migration for both low (Fig. 2g,  $p=0.65$ ) and high (Fig. 2h,  $p=0.08$ ) injection doses. To control for a potential interaction between CFSE and PFC, the exact same experiment was conducted using DsRed<sup>+</sup> BMDC transgenic mice. No statistical difference in *in vivo* migration of PFC-labeled and unlabeled DsRed<sup>+</sup> BMDC was observed (Fig. 2i,  $p=0.43$ ).

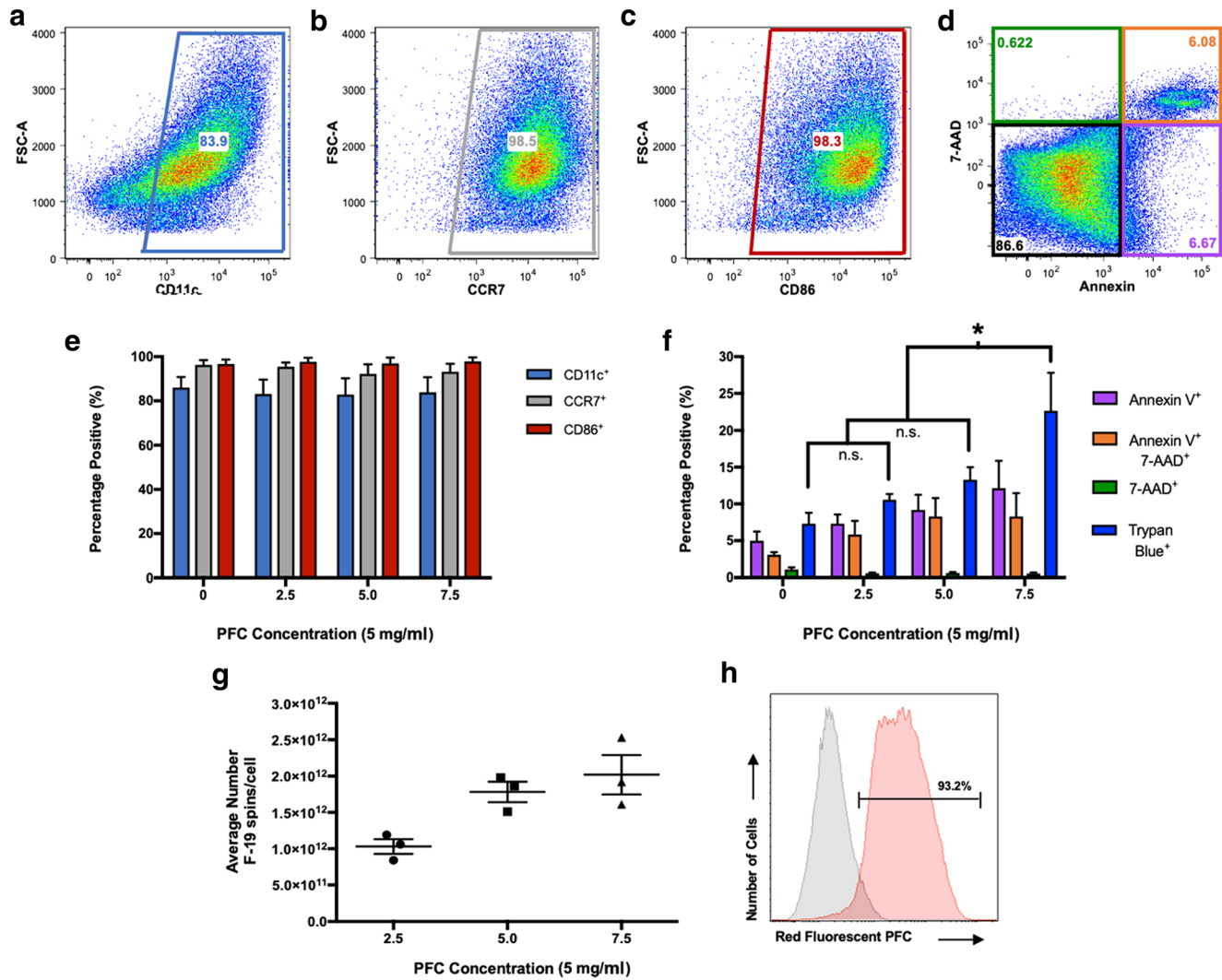


**Fig. 1.** CD11c<sup>+</sup> BMDC label with PFC without affecting viability and phenotype. **a** CD11c<sup>+</sup> BMDC were phenotyped for **b** CCR7 and **c** CD86 expression and then viability assessed using **d** Annexin V/7-AAD. **e** BMDC phenotype and **f** viability were determined across PFC concentrations. PFC labeling of BMDC occurred in **g** dose-dependent manner, with **h** > 90 % of CD11c<sup>+</sup> BMDC incorporating fluorescent PFC label. Data shown as mean  $\pm$  SEM (two-way ANOVA, \* $p$  < 0.05).

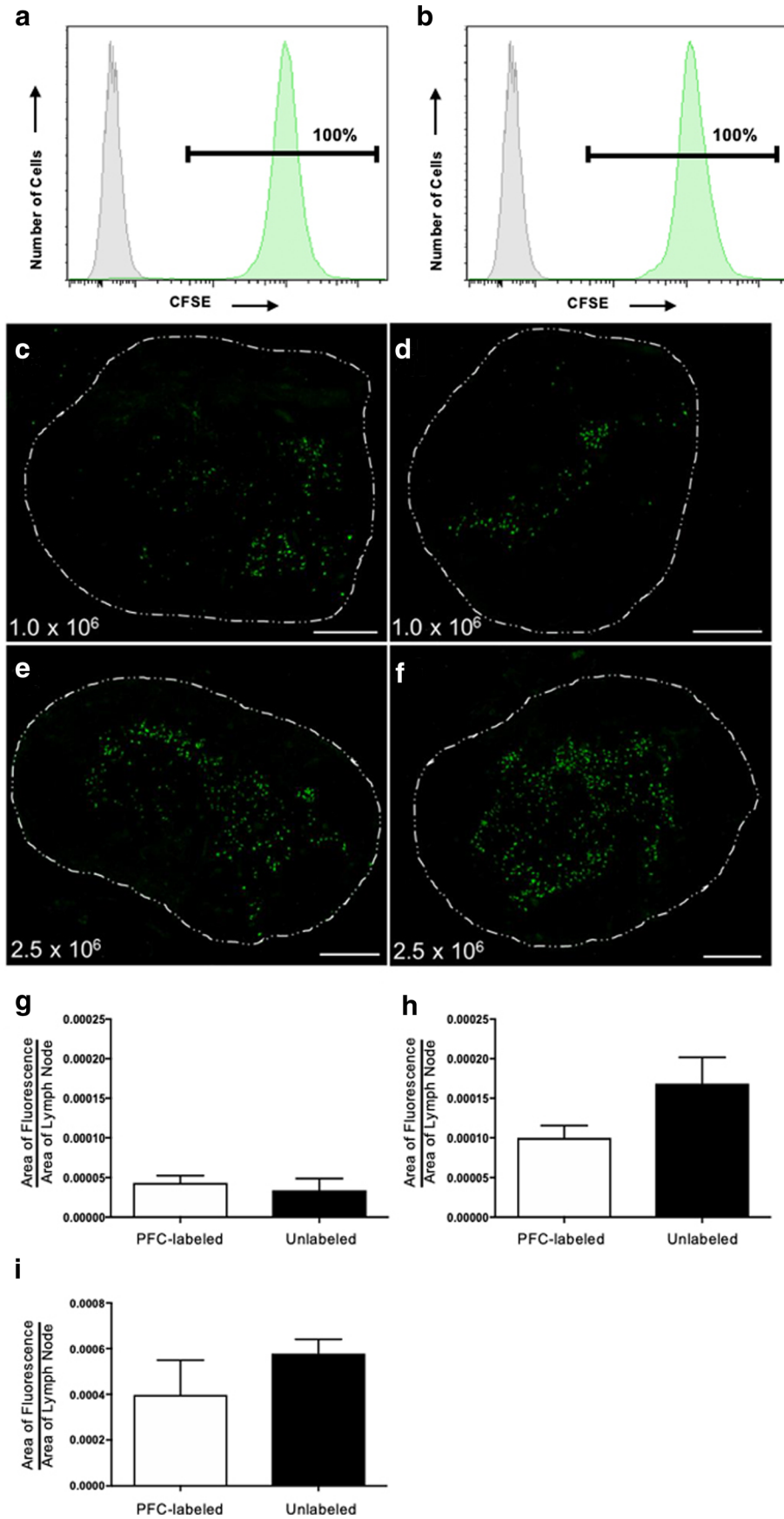
### *F-19 Cellular MRI Detection of PFC-Labeled BMDC Migration to the Popliteal Lymph Node*

We next investigated if F-19 cellular MRI was suitable to detect increases in BMDC *in vivo* migration as a result of lymph node pre-treatment with IL-1 $\beta$  (300 ng). Three hours after popliteal lymph node IL-1 $\beta$  pre-treatment of four mice,  $3 \times 10^6$  PFC-labeled BMDC were injected into both hind footpads. A separate group of three mice received the same injections without IL-1 $\beta$  pre-treatment. F-19 MRI was performed 2 days later and PFC-labeled BMDC produced a quantifiable footpad and popliteal lymph node F-19 signal (Fig. 3a). IL-1 $\beta$  pre-treated mice (mouse 1–4) had quantifiable migration in five of eight popliteal lymph nodes (range  $4000 \pm 800$  to  $20,000 \pm 3000$  cells) while mice not receiving IL-1 $\beta$  pre-treatment (mouse 5–7) had quantifiable BMDC migration in four of six popliteal lymph nodes (range  $4300 \pm 600$  to  $17,000 \pm 2000$  cells, Fig. 3a, absence of

quantifiable signal denoted by [\*]). PFC-labeled BMDC quantification for both conditions revealed that IL-1 $\beta$  pre-treatment only tended to increase *in vivo* migration (Fig. 3b).

**Fig. 2.** PFC does not impede BMDC *in vivo* migration. **a** CFSE<sup>+</sup> PFC-labeled BMDC and **b** CFSE<sup>+</sup> control BMDC were formulated into low ( $1 \times 10^6$ ) and high ( $2.5 \times 10^6$ ) hind footpad injection doses ( $n = 7$  per dose). Two days later, images of popliteal lymph node cryosections revealed CFSE fluorescence for **c** low and **e** high PFC-labeled BMDC injection doses and **d** low and **f** high control BMDC injection doses, respectively. CFSE fluorescence quantification is summarized for **g** low and **h** high injection conditions. **i** The same experiment was conducted and quantified with  $2 \times 10^6$  DsRed<sup>+</sup> PFC-labeled or control BMDC injections ( $n = 4$  mice). The experimenter was blinded prior to image acquisition, images were taken at  $\times 100$  magnification (scale bar = 300  $\mu$ m) and data shown as mean  $\pm$  SEM ( $t$  test,  $p > 0.05$ ).





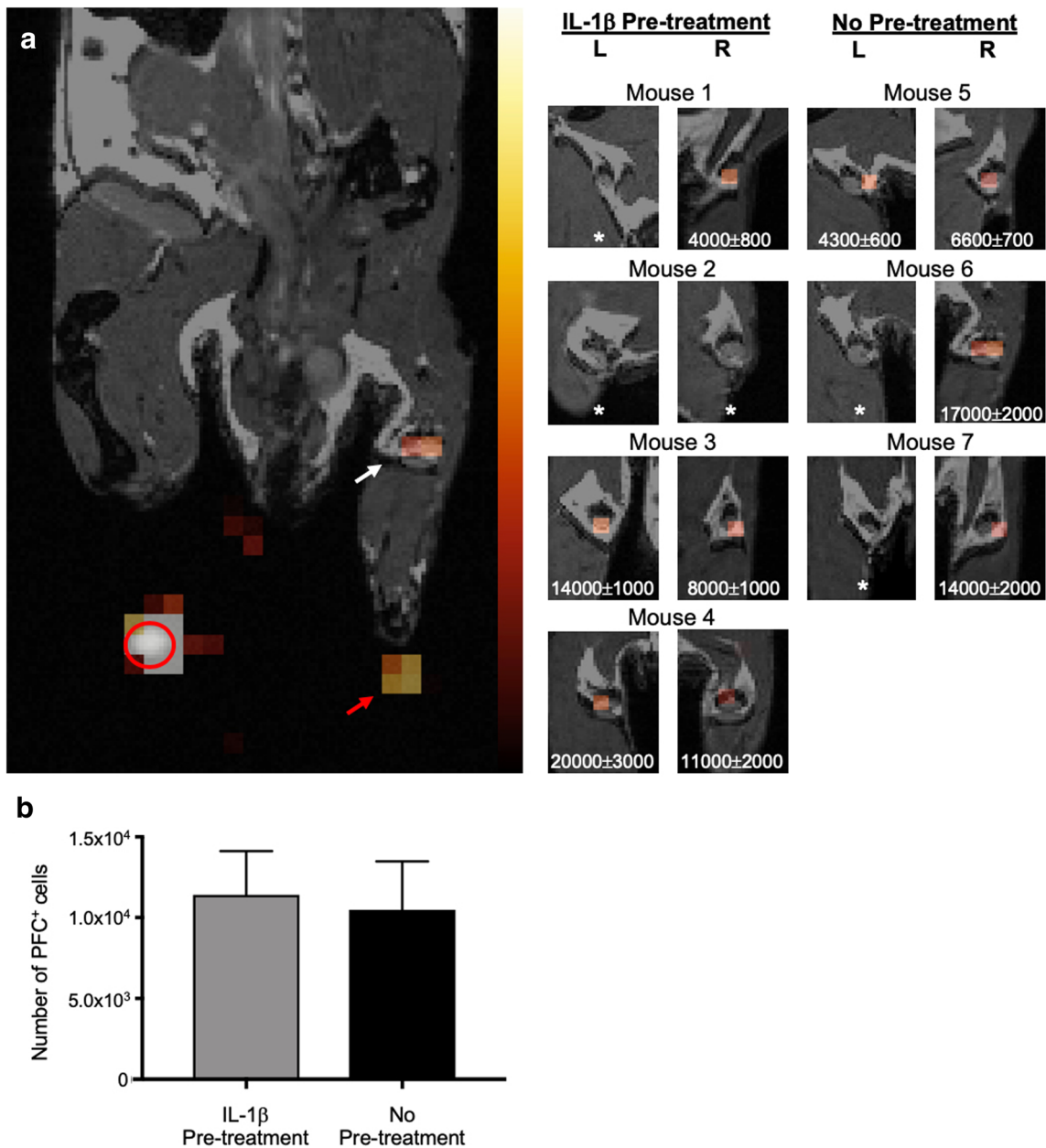


**Fig. 3.** F-19 MRI detection and quantification of BMDC migration to popliteal lymph nodes. PFC-labeled BMDC ( $3 \times 10^6$ ) hind footpad injections were performed on mice that received left (L) and right (R) popliteal lymph node area IL-1 $\beta$  (300 ng) pre-treatment 3 h earlier (mouse 1–4), while mouse 5–7 did not receive pre-treatment. **a** A representative 9.4 T proton/F-19 MRI composite identified F-19 signal (“hot-iron” pseudocolored) at the injection site (red arrow), popliteal lymph node (white arrow), and reference tube (red circle) 2 days later. Popliteal lymph node composites for each mouse are shown with quantifiable signal in white text and lack of quantifiable signal denoted by asterisk (\*). **b** The average number of MRI-detectable BMDC that migrate to a target lymph node is displayed for both injection conditions (means  $\pm$  SEM). Data is representative of  $N=2$  independent experiments, with  $n=3-4$  mice per condition ( $t$  test,  $p > 0.05$ ).

### *PFC Labeling Does Not Interfere with BMDC Induction of an Antigen-Specific Immune Response*

The ability of PFC-labeled BMDC to present antigen and initiate an antigen-specific immune response was compared to unlabeled BMDC presenting the same antigen, while

antigen-unloaded unlabeled BMDC served as the negative control. BMDC exhibited a mature phenotype as described in Fig. 1 for all three conditions. Additional gating for H-2K<sup>b</sup> demonstrated that nearly all CD11c<sup>+</sup>CD86<sup>+</sup>CCR7<sup>+</sup> BMDC were H-2K<sup>b</sup><sup>+</sup>. Surface presentation of SIINFEKL (OVA<sub>257-264</sub>) in the context of H-2K<sup>b</sup> was measured with an antibody specifically recognizing H-2K<sup>b</sup>:SIINFEKL

complex [21] with non-specific background levels detected (<2 %) for the negative control formulation (Fig. 4a). This was in stark contrast to >98 % of BMDC positive for SIINFEKL:H-2K<sup>b</sup> complex after a 2-h incubation with SIINFEKL peptide for control unlabeled (Fig. 4b) and

PFC-labeled (Fig. 4c) BMDC. Hence, PFC did not interfere with MHC Class I expression nor loading of SIINFEKL onto surface-expressed H-2K<sup>b</sup> molecules.

Unlabeled control BMDC and PFC-labeled BMDC (both presenting SIINFEKL peptide) were injected into both hind

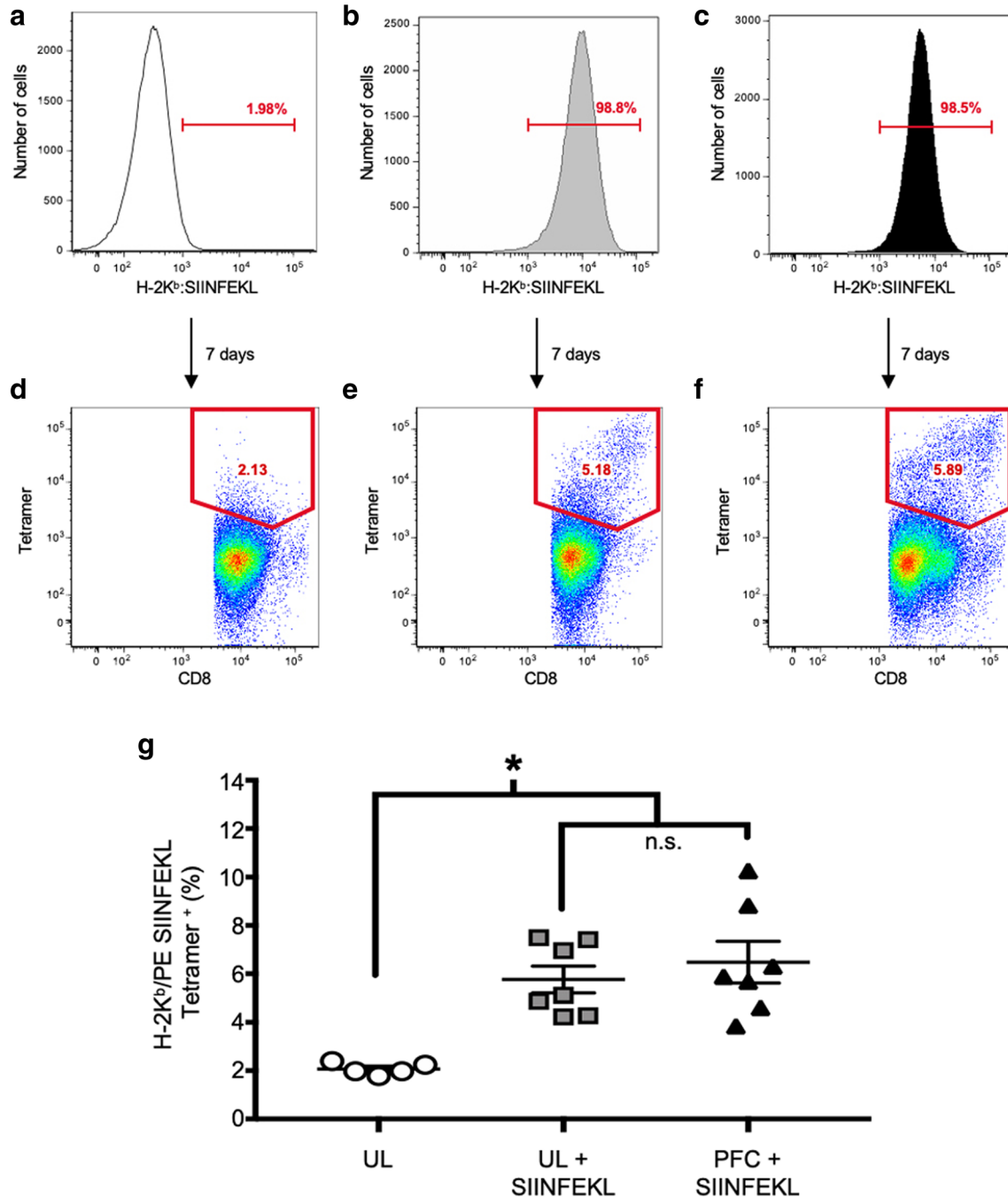


**Fig. 4.** BMDC-induced antigen-specific immune response is unaffected by PFC labeling. **a** BMDC not incubated with SIINFEKL peptide have low non-specific H-2K<sup>b</sup>:SIINFEKL complex staining compared to >98 % staining observed for **b** control and **c** PFC-labeled BMDC incubated with SIINFEKL peptide. **d-f** One week after  $3 \times 10^6$  BMDC hind footpad injections were performed for each injection condition, single cell suspension from excised popliteal lymph nodes were analyzed to identify CD3<sup>+</sup>CD8<sup>+</sup> T cells that express a TCR that specifically binds H-2K<sup>b</sup>:SIINFEKL. SIINFEKL-specific CD8<sup>+</sup> T cell immune responses are summarized for **g** all three injection conditions described in (a-c). Data is representative of  $N=4$  independent experiments ( $n=5-7$  mice in each group) and is shown as mean  $\pm$  SEM (one-way ANOVA, \* $p < 0.05$ ).

footpads of seven mice per condition ( $2.5 \times 10^6$ ). Five negative control mice received unlabeled BMDC not presenting peptide. SIINFEKL-specific CD8<sup>+</sup> T cell immune responses developed in the draining popliteal lymph nodes for 1 week. Subsequently, both popliteal lymph nodes were removed and processed for each mouse to identify CD3<sup>+</sup>CD8<sup>+</sup> T cells whose T cell receptor (TCR) specifically recognizes the SIINFEKL peptide:H-2K<sup>b</sup> complex *via* tetramer staining (Fig. 4d–f). Similar percentages of tetramer<sup>+</sup> CD3<sup>+</sup>CD8<sup>+</sup> T cells were measured for PFC-labeled and control BMDC conditions, indicating that PFC does not interfere with BMDC induction of antigen-specific immune responses *in vivo*. Both were significantly higher than the background immune response observed in the negative control condition (Fig. 4g).

### *F-19 Cellular MRI Detection of PFC-Labeled BMDC in Tumor-Bearing C57BL/6 Mice*

We engineered a B16-F10 melanoma cell line to express ovalbumin (OVA), green fluorescent protein (GFP), and luciferase (luc). This luc<sup>+</sup>GFP<sup>+</sup>OVA<sup>+</sup> cell line (B16-F10<sup>+++</sup>, Online Resource 1) was used in a tumor-bearing mouse challenge experiment (Fig. 5a) to address whether PFC labeling affected BMDC migration and tumor therapy outcome. BMDC were confirmed mature and SIINFEKL peptide-presenting as described in Figs. 1 and 4, respectively, prior to immunization and did not differ between injection conditions (Fig. 5b). Greater than 90 % of cells surface express SIINFEKL:H-2K<sup>b</sup> for both for control BMDC ( $91.0 \pm 2.02$  %) and PFC-labeled BMDC ( $93.6 \pm 0.38$  %) incubated with SIINFEKL (Fig. 5b). Negative control BMDC revealed only background non-specific SIINFEKL:H-2K<sup>b</sup> staining (Fig. 5b). Moreover, the intensity of SIINFEKL peptide surface presentation (determined by MFI) did not significantly differ between SIINFEKL-presenting control, unlabeled BMDC (MFI =  $3103 \pm 508$ ), and PFC-labeled BMDC (MFI =  $2195 \pm 314$ ) preparations (Fig. 5c,  $p = 0.23$ ) and was above the threshold required for inducing a SIINFEKL-specific immune response.

All C57BL/6 mice were inoculated with  $7 \times 10^4$  B16-F10<sup>+++</sup> cells (day minus 2 (day -2)) and then immunized in both hind footpads with  $3 \times 10^6$  BMDC (designated day 0) from one of the three aforementioned injection conditions ( $n = 4$ –5 mice per condition). PFC-labeled BMDC-injected tumor-bearing mice underwent proton/F-19 MRI at 3 T on day 2 after immunization. A representative overlay of an anatomical MRI with pseudocolored F-19 MRI demonstrated that PFC-labeled BMDC produced quantifiable F-19 signal in the left and right popliteal lymph nodes (Fig. 5d). A F-19 signal was also detected in both hind footpad injection sites (range  $1.24$ – $1.60 \times 10^6$  cells, Fig. 5d). Left and right popliteal lymph node area insets for all mice that received PFC-labeled BMDC vaccinations are shown (Fig. 5d) and color-matched with

the popliteal lymph node quantification (Fig. 5e). PFC-labeled cells were detected in all but one popliteal lymph node and ranged from  $3.63 \times 10^3$  to  $1.91 \times 10^4$  cells.

B16-F10<sup>+++</sup> tumor-bearing mice were longitudinally analyzed *via* bioluminescence imaging (BLI) and a Vernier caliper to monitor tumor growth (Fig. 6a). The fold change in BLI signal from day 0 (Fig. 5a) was graphed for each immunization condition until experimental endpoint, with larger tumors associated with negative control immunizations compared to SIINFEKL-presenting control BMDC and SIINFEKL-presenting PFC-labeled BMDC immunizations (Fig. 6b). A survival analysis, represented using the same color scheme in Fig. 6a/b, suggests extended and equivalent survival (~6 days) for both SIINFEKL-presenting BMDC immunizations in 30 % of the mice (Fig. 6c). PFC labeling of SIINFEKL-presenting BMDC permits detection and quantification of *in vivo* migration to popliteal lymph nodes using F-19 cellular MRI without affecting the ensuing SIINFEKL-specific anti-tumor response occurring in tumor-bearing mice compared to SIINFEKL-presenting control BMDC immunizations.

## Discussion

When compared to more widely used iron oxide-based MRI, F-19 is much less sensitive; however, it is becoming increasingly popular due to the important advantages it has over conventional cellular MRI employing contrast agents. F-19 MRI sensitivity is dependent on intracellular F-19 concentration, MR properties of the F-19 label, and MRI system hardware and acquisition parameters [22, 23], all of which contribute to potential low signal-to-noise ratio (SNR). To compensate, F-19 signal is strengthened by imaging at magnetic field strengths well above 3 T [24, 25]. With clinical translation in mind, our group used a surface coil and SNR-efficient bSSFP pulse sequence to detect and quantify tumor-associated macrophages [26] and migrated BMDC presented here in mice at 3 T, the maximum field strength for most human MRI systems. By translating F-19 MRI into the clinical realm, PFC-labeled therapeutic cells can be unambiguously detected and quantified *in vivo* due to the lack of endogenous F-19. This is in stark contrast to iron oxide-based MRI, which produces a negative contrast signal void or blooming artifact indistinguishable from chemical shift artifacts originating from anatomical structures like high fat-tissue interfaces, air-filled lungs, and iron-rich blood vessels and spleen [15, 27].

### *PFC Labeling Does Not Alter BMDC Viability, Phenotype, and In Vivo Migration*

To combat low sensitivity of F-19 detection, preliminary studies centered around culture conditions that produced maximal PFC uptake. Culturing highly endocytic, immature BMDC with 5.0 mg/ml PFC resulted in efficient PFC



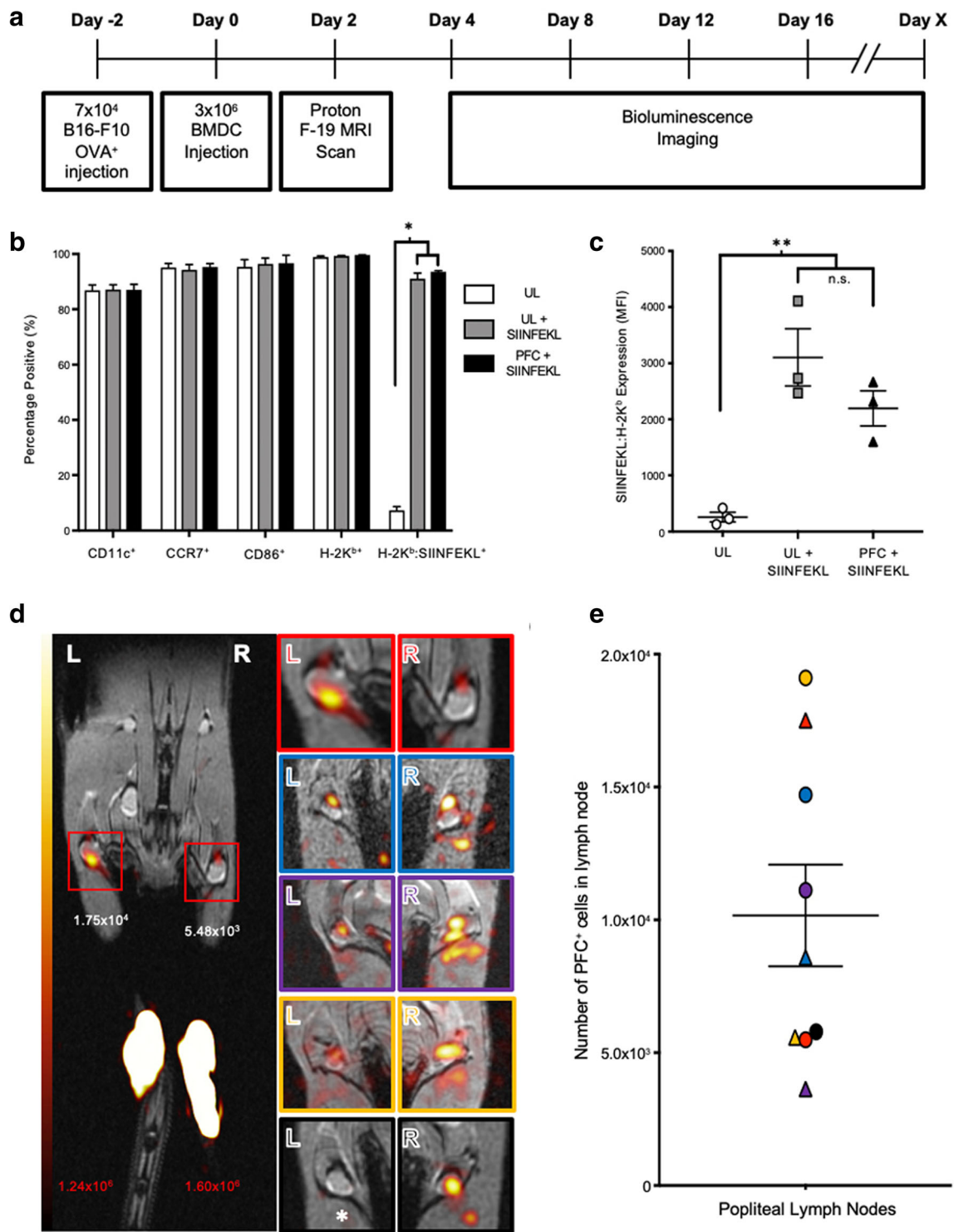


**Fig. 5.** F-19 MRI detection of BMDC migration to the popliteal lymph node in B16-F10<sup>+++</sup> tumor-bearing mice. **a** C57BL/6 mice received BMDC immunizations (described in Fig. 4) 2 days after B16-F10<sup>+++</sup> inoculation. **b** BMDC phenotype and **c** MFI did not differ between injection conditions except for H-2K<sup>b</sup>:SIINFEKL complex, in which control and PFC-labeled BMDC incubated with SIINFEKL had significantly increased percentage positive and elevated MFI of H-2K<sup>b</sup>:SIINFEKL BMDC compared to BMDC not incubated with SIINFEKL (gray, black compared to white bars/symbols). **d** Proton/F-19 MRI (3 T) overlay reveals injection site (red text) and popliteal lymph node (red boxes) F-19 detection 2 days after injection as well as popliteal lymph node composites for each mouse. **e** Lymph node-migrated BMDC were quantified (triangles = left lymph nodes, circles = right lymph nodes) for all nodes but one (denoted by asterisk (\*), **d**). Data shown as mean ± SEM (two-way ANOVA, \**p* < 0.05, one-way ANOVA, \*\**p* < 0.05).

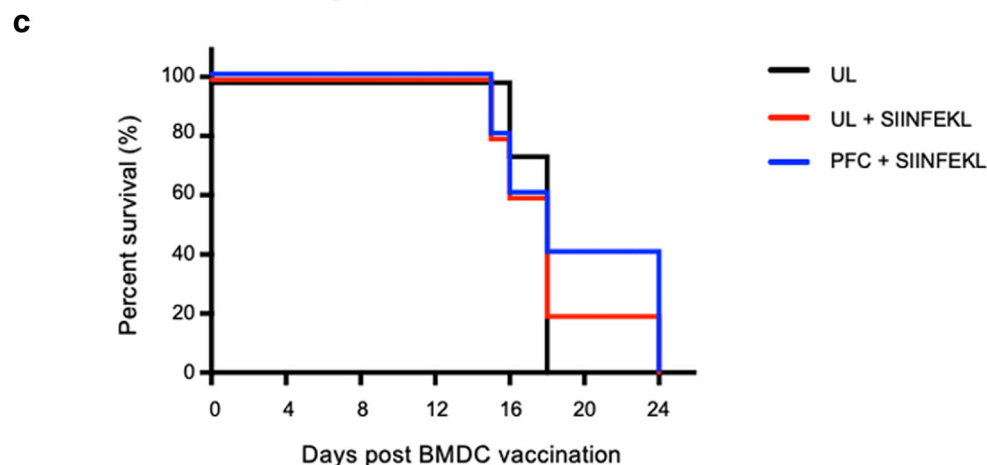
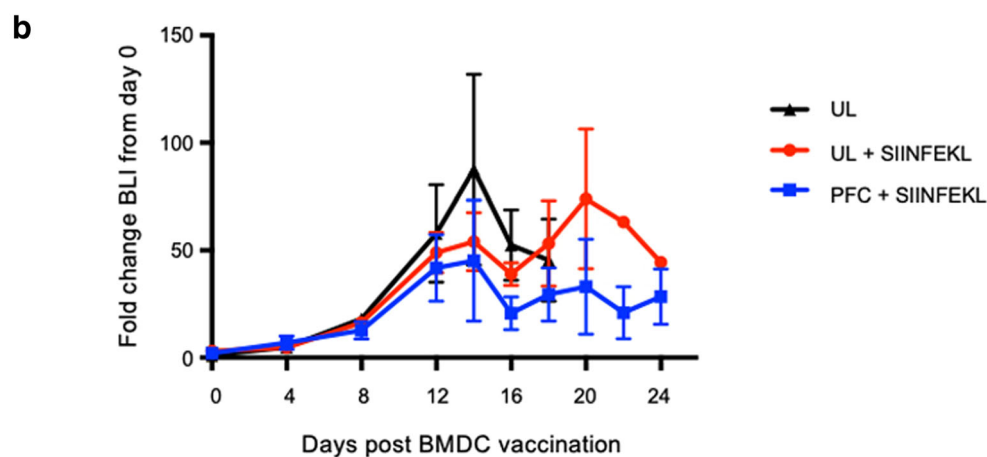
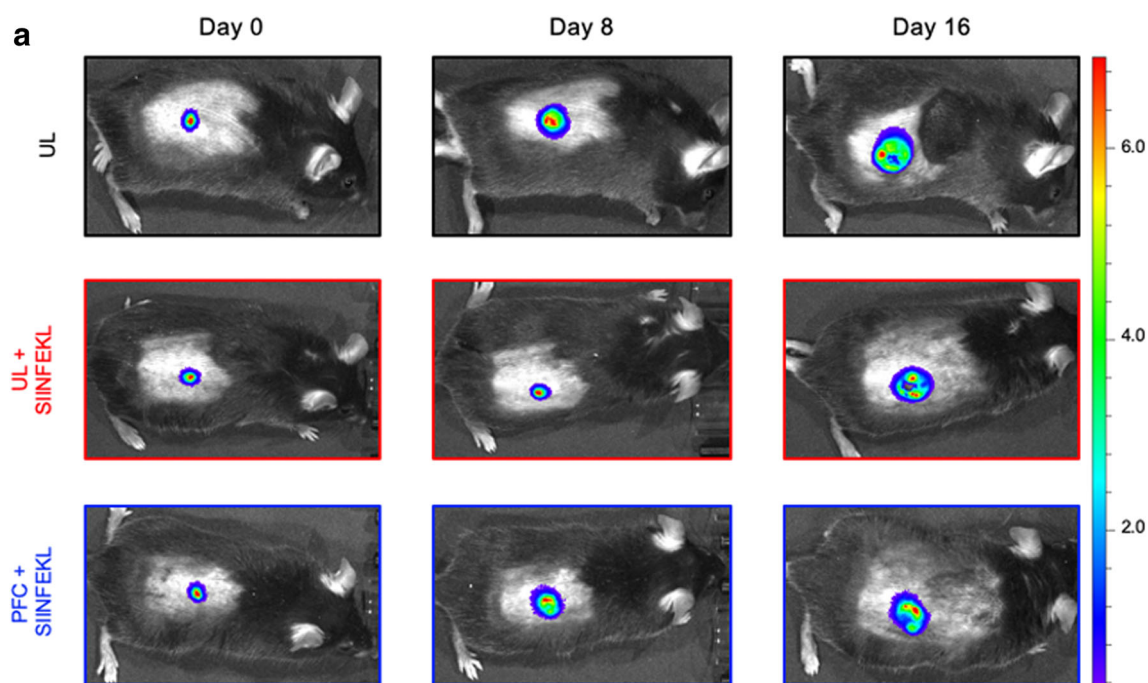


Fig. 6. Anti-tumor immune response induced by BMDC immunization is unaffected by PFC labeling in tumor-bearing mice. Tumor growth was monitored with **a** BLI (radiance ( $p/s/cm^2/sr \times 10^7$ ) scale on right) and **b** measured longitudinally (fold change from day 0 BLI measurement). **c** A Kaplan-Meier survival analysis is displayed for mice that received BMDC not presenting SIINFEKL (black), control BMDC presenting SIINFEKL (red), and PFC-labeled BMDC presenting SIINFEKL (blue). Data shown as mean  $\pm$  SEM.

loading ( $1.783 \times 10^{12}$  F-19 spins/cell) while BMDC phenotype or viability remained unchanged. Any further increases in PFC concentration were associated with modest improvements to PFC uptake at the detriment of significant decreases in viability. Both PFC loading and decreased viability with increasing PFC concentration are consistent with previous reports [16, 28, 29]. A red fluorescent version of PFC was employed to qualitatively assess label uptake *via* flow cytometric analysis. Greater than 93 % of CD11c<sup>+</sup> BMDC incorporated PFC, which is far superior than BMDC labeling efficiencies ( $43.9 \pm 17.4$  %) reported with the positron emission tomography (PET) agent, [<sup>89</sup>Zr]Oxine [30], for example.

For DC to function as adjuvants in cell-based cancer immunotherapies, they must be *in vivo* migration-competent and possess a mature and activated phenotype. Without such attributes, tumor-induced immunosuppression is not overcome and the potential for induction of a tolerogenic rather than effective TAA-specific immune response exists [31, 32]. We do not consider this to be an issue in our model due to equivalent and high surface expression of CD86 and CCR7 measured for both BMDC conditions. In demonstrating that PFC-labeled and unlabeled BMDC migration to a draining lymph node does not significantly differ, we are the first to report on the comparison of PFC-labeled and unlabeled therapeutic cell migration, rather than simply reporting therapeutic cells are migration-competent after PFC labeling [11]. Additionally, unlike SPIO-labeled BMDC that are susceptible to varying degrees of impaired migration based on SPIO size [14, 33], PFC-labeled BMDC do not exhibit such an impairment. Within secondary lymphoid paracortical regions, BMDC present TAA in association with appropriate co-stimulatory and cytokine signaling that leads to *de novo* activation and proliferation of TAA-specific CTL, which is absolutely required for DC-based immunotherapeutic benefit.

### *Detection and Quantification of PFC-Labeled BMDC In Vivo Migration Using F-19 MRI*

For F-19 cellular MRI to serve as a surrogate non-invasive marker of DC-based immunotherapeutic effectiveness, quantifiable F-19 signal in the lymph node from PFC-labeled BMDC must be possible [34]. We used an established method to increase BMDC migration [5, 35] by treating the draining popliteal lymph node area with IL-1 $\beta$  prior to BMDC adoptive transfer as a main contributor to suboptimal immunotherapeutic success is the low percentage of DC that reach the lymph node post injection [10]. With our 9.4 T small animal MR scanner system, quantifiable PFC-labeled BMDC signal was measured, but an IL-1 $\beta$ -induced enhanced migration was not observed. Due to the low sensitivity of F-19 MRI,  $3 \times 10^6$  PFC-labeled BMDC were adoptively transferred to ensure quantifiable *in vivo* F-19 signal detection. Tissue pre-conditioning functions best at

low injection doses [36] and thus, we believe that this injection dose was too high to detect measurable increases in migration due to tissue pre-conditioning. Even so, demonstrating consistent detection of lymph node-migrated PFC-labeled BMDC using F-19 MRI in combination with fluorescence microscopy detection of CFSE<sup>+</sup> and DsRed<sup>+</sup> BMDC in the lymph node permits our group to conclude that *in vivo* F-19 signal is primarily due to originally injected migration-competent PFC-labeled BMDC. This is further strengthened by previous xenogeneic work from our laboratory in which murine lymph nodes with detectable F-19 MRI signal were digested and counterstained with human CD45 to select for CFSE<sup>+</sup> CD45<sup>+</sup> originally injected human PBMC [18]. The identification of human CD45<sup>+</sup> cells in lymph nodes eliminates the notion of false positive signal caused by resident murine macrophages engulfing apoptotic PFC-labeled cells [37]. Lastly, migration to alternative *in vivo* locations (liver, spleen, and lungs) most likely occurred, albeit it at a level below the detection threshold. PFC is stably retained within live cells but is rapidly cleared *via* the reticuloendothelial system [38] and eventually by the lungs following cell apoptosis.

### *Labeling BMDC with PFC Does Not Hinder In Vivo Antigen-Specific Immune Response*

Although DC TAA presentation in secondary lymphoid organs initiates a cascade of events resulting in broad innate and adaptive immune cell activation [2, 3], quantification of TAA-specific CD8<sup>+</sup> T cell activation is widely used to assess anti-tumor immune responses [39]. Therefore, a H-2K<sup>b</sup>-restricted immunogenic epitope, derived from chicken ovalbumin, SIINFEKL (OVA<sub>257-264</sub>), served as a model pseudo-TAA presented in the context of H-2K<sup>b</sup> on nearly 100 % of PFC-labeled and unlabeled BMDC. Seven days after immunization when T cell-mediated responses are highest [40], SIINFEKL-specific CD8<sup>+</sup> T cell responses were measured in popliteal lymph nodes. The magnitude of TAA-specific response was unchanged by PFC labeling of therapeutic BMDC and was significantly higher than background levels measured in the negative control condition, indicating that a productive SIINFEKL-specific immune response was launched. This provides further validation that lymph node-migrated BMDC are viable and capable of initiating an immune response, and that with our current setup, PFC-labeled BMDC *in vivo* migration can be quantified with F-19 MRI without affecting viability, phenotype, and function.

### *Monitoring PFC-Labeled BMDC Migration in a Tumor-Bearing Mouse Model*

The highly immunosuppressive and metastatic cell line, B16-F10 [41], was chosen for our C57BL/6 tumor-bearing mouse model as prior murine studies have noted both cell-

and humoral-mediated anti-tumor immune responses [42, 43]. Following subcutaneous B16-F10 inoculation, mice were immunized with SIINFEKL-presenting PFC-labeled BMDC that were migration-competent as detected and quantified with F-19 MRI. With continuous monitoring of tumor growth by BLI and caliper measurement alongside survival analysis, slower tumor growth and thus, prolonged survival, was observed in 20–40 % of tumor-bearing mice that received SIINFEKL-presenting PFC-labeled or unlabeled BMDC immunizations compared to control mice (day 24 *versus* day 18, respectively). We acknowledge that the modest immunotherapeutic effect is based on a small number of animals and not really an indication of efficacy; however, our current tumor-bearing mouse model is conducive to characterizing PFC-labeled BMDC migration and serving as a non-invasive image modality to assess immunotherapeutic effectiveness.

The suboptimal immunotherapeutic efficacy described above has several possible explanations. The maturation cocktail used to mature BMDC *ex vivo* contains prostaglandin E<sub>2</sub> (PGE<sub>2</sub>) in order to activate CCR7 and render BMDC *in vivo* migration-competent [44]. PGE<sub>2</sub> has also been shown to limit BMDC-derived IL-12 secretion. Together with IFN- $\gamma$ , IL-12 promotes T<sub>H</sub>1-mediated CD4<sup>+</sup> T helper (T<sub>H</sub>) cell immune responses that are required for long-term CTL responses to persist [3, 44]. Caution with drawing conclusions regarding PGE<sub>2</sub> inclusion in BMDC generation should be exercised as PFC-labeled and unlabeled BMDC both up-regulated CD40 upon maturation cocktail stimulation (data not shown). This is consistent with previous reports from our group and leads to enhanced and prolonged IL-12 secretion upon ligation with CD154 [3, 20, 33] present on CD4<sup>+</sup> T<sub>H</sub> cells.

By demonstrating a strong induction of SIINFEKL-specific CD8<sup>+</sup> T cell responses in tumor-naïve mice yet marginal immunotherapeutic benefit for the same immunization in tumor-bearing mice, it is likely that B16-F10<sup>+++</sup> tumor-induced immunosuppression and rapid growth contributed to this disparity. An immunosuppressive tumor microenvironment is established by but not limited to secretion of transforming growth factor- $\beta$ , vascular endothelial growth factor, and IL-10 that, in turn, recruit and retain myeloid-derived suppressor cells and regulatory CD4<sup>+</sup> T cells [45, 46]. In combination with H-2K<sup>b</sup> down-regulation, overcoming tumor-induced immunosuppression is challenging and tumor-penetrating immune cells develop an exhaustion rather than effector phenotype [45]. In our model, we do not believe H-2K<sup>b</sup> down-regulation to be the primary culprit as nearly all tumor cells surface-expressed H-2K<sup>b</sup> prior to inoculation. Moreover, immune responses directed at TAA, such as human tyrosinase-related protein-2, have been launched in the presence of tumor-induced H-2K<sup>b</sup> down-regulation [47]. A more robust phenotypic comparison of markers of activation (CD44, CD69, CD137), degranulation (LAMP-1), and exhaustion (PD-1) [46, 48] of TAA-specific CTL between tumor-naïve and tumor-bearing mice would provide useful mechanistic information pertaining to the lack of greater anti-tumor efficacy.

## Conclusions

This is the first report demonstrating that PFC does not significantly impede *in vivo* BMDC migration or interfere with BMDC functionality in the context of cell-based immunotherapies. F-19 cellular MRI is a useful and non-invasive imaging modality to compare *in vivo* migration and thus, immunotherapeutic potency, between differing BMDC generation protocols, such as inclusion of poly(I:C), a toll-like receptor (TLR)3 ligand, within the maturation cocktail [42]. F-19 MRI is also broadly amenable as a surrogate marker to compare immunotherapeutic efficacies of combination therapies, an example being DC-based immunotherapies and checkpoint inhibitors that have proven effective in combating melanoma [49]. Finally, F-19 MRI can be exploited to gain knowledge regarding *in vivo* migration of therapeutic cells in emerging small animal models, like the tamoxifen-induced mouse model of human melanoma [50], as well as in different immunogenic tumors and disease states.

*Acknowledgments.* We thank Dr. Amanda Hamilton and Dr. Kristin Chadwick for technical expertise and Dr. Thomas Craig Meagher for assistance with manuscript reviewing.

*Funding Information.* This research was supported by a grant from the Ontario Institute for Cancer Research.

### Compliance with Ethical Standards

### Conflict of Interest

The authors declare that they have no conflict of interest.

## References

- Gerritsen WR (2012) The evolving role of immunotherapy in prostate cancer. *Ann Oncol* 23(Suppl 8):viii22–viii27
- Schreibelt G, Benitez-Ribas D, Schuurhuis D et al (2010) Commonly used prophylactic vaccines as an alternative for synthetically produced TLR ligands to mature monocyte-derived dendritic cells. *Blood* 116:564–574
- Waldmann TA (2018) Cytokines in cancer immunotherapy. *Cold Spring Harb Perspect Biol* 10:
- Forster R, Braun A, Worbs T (2012) Lymph node homing of T cells and dendritic cells via afferent lymphatics. *Trends Immunol* 33:271–280
- Martin-Fontecha A, Sebastiani S, Hopken UE et al (2003) Regulation of dendritic cell migration to the draining lymph node: impact on T lymphocyte traffic and priming. *J Exp Med* 198:615–621
- Wang B, Sun C, Wang S et al (2018) Mouse dendritic cell migration in abdominal lymph nodes by intraperitoneal administration. *Am J Transl Res* 10:2859–2867
- Scheid E, Major P, Bergeron A et al (2016) Tn-MUC1 DC vaccination of rhesus macaques and a phase I/II trial in patients with nonmetastatic castrate-resistant prostate cancer. *Cancer Immunol Res* 4:881–892
- Blalock LT, Landsberg J, Messmer M et al (2012) Human dendritic cells adenovirally-engineered to express three defined tumor antigens promote broad adaptive and innate immunity. *Oncoimmunology* 1:287–357
- Butterfield LH (2013) Dendritic cells in cancer immunotherapy clinical trials: are we making progress? *Front Immunol* 4:454
- Verdijk P, Aarntzen EH, Lesterhuis WJ et al (2009) Limited amounts of dendritic cells migrate into the T-cell area of lymph nodes but have



- high immune activating potential in melanoma patients. *Clin Cancer Res* 15:2531–2540
11. Ahrens ET, Helfer BM, O'Hanlon CF, Schirda C (2014) Clinical cell therapy imaging using a perfluorocarbon tracer and fluorine-19 MRI. *Magn Reson Med* 72:1696–1701
  12. Gaudet JM, Ribot EJ, Chen Y et al (2015) Tracking the fate of stem cell implants with fluorine-19 MRI. *PLoS One* 10:e0118544
  13. Dekaban GA, Hamilton AM, Fink CA et al (2013) Tracking and evaluation of dendritic cell migration by cellular magnetic resonance imaging. *Wires Nanomed Nanobi* 5:469–483
  14. Rohani R, de Chickera SN, Willert C et al (2011) In vivo cellular MRI of dendritic cell migration using micrometer-sized iron oxide (MPIO) particles. *Mol Imaging Biol* 13:679–694
  15. Dekaban GA, Snir J, Shrum B et al (2009) Semiquantitation of mouse dendritic cell migration in vivo using cellular MRI. *J Immunother* 32:240–251
  16. Bonetto F, Srinivas M, Heerschap A et al (2011) A novel <sup>19</sup>F agent for detection and quantification of human dendritic cells using magnetic resonance imaging. *Int J Cancer* 129:365–373
  17. Chapelin F, Capitini CM, Ahrens ET (2018) Fluorine-19 MRI for detection and quantification of immune cell therapy for cancer. *J Immunother Cancer* 6:105
  18. Fink C, Gaudet JM, Fox MS et al (2018) <sup>19</sup>F-perfluorocarbon-labeled human peripheral blood mononuclear cells can be detected in vivo using clinical MRI parameters in a therapeutic cell setting. *Sci Rep* 8:590
  19. Inaba K, Inaba M, Romani N et al (1992) Generation of large numbers of dendritic cells from mouse bone marrow cultures supplemented with granulocyte/macrophage colony-stimulating factor. *J Exp Med* 176:1693–1702
  20. de Chickera S, Willert C, Mallet C et al (2012) Cellular MRI as a suitable, sensitive non-invasive modality for correlating in vivo migratory efficiencies of different dendritic cell populations with subsequent immunological outcomes. *Int Immunol* 24:29–41
  21. Sethumadhavan S, Silva M, Philbrook P et al (2017) Hypoxia and hypoxia-inducible factor (HIF) downregulate antigen-presenting MHC class I molecules limiting tumor cell recognition by T cells. *PLoS One* 12:e0187314
  22. Srinivas M, Boehm-Sturm P, Figdor CG et al (2012) Labeling cells for in vivo tracking using <sup>19</sup>F MRI. *Biomaterials* 33:8830–8840
  23. Taylor AJ, Granwehr J, Lesbats C et al (2016) Probe-specific procedure to estimate sensitivity and detection limits for <sup>19</sup>F magnetic resonance imaging. *PLoS One* 11:e0163704
  24. Srinivas M, Morel PA, Ernst LA et al (2007) Fluorine-19 MRI for visualization and quantification of cell migration in a diabetes model. *Magn Reson Med* 58:725–734
  25. Hitchens TK, Ye Q, Eytan DF et al (2011) <sup>19</sup>F MRI detection of acute allograft rejection with in vivo perfluorocarbon labeling of immune cells. *Magn Reson Med* 65:1144–1153
  26. Makela AV, Foster PJ (2018) Pre-clinical <sup>19</sup>F MRI cell tracking at 3 Tesla. *Magma*
  27. Long CM, van Laarhoven HW, Bulte JW, Levitsky HI (2009) Magnetovaccination as a novel method to assess and quantify dendritic cell tumor antigen capture and delivery to lymph nodes. *Cancer Res* 69:3180–3187
  28. Srinivas M, Tel J, Schreiber G et al (2015) PLGA-encapsulated perfluorocarbon nanoparticles for simultaneous visualization of distinct cell populations by <sup>19</sup>F MRI. *Nanomedicine (London)* 10:2339–2348
  29. Bouchlaka MN, Ludwig KD, Gordon JW et al (2016) <sup>19</sup>F-MRI for monitoring human NK cells in vivo. *Oncoimmunology* 5:e1143996
  30. Sato N, Wu H, Asiedu KO et al (2015) <sup>89</sup>Zr-oxine complex PET cell imaging in monitoring cell-based therapies. *Radiology* 275:490–500
  31. Wimmers F, Schreiber G, Skold AE et al (2014) Paradigm shift in dendritic cell-based immunotherapy: from in vitro generated monocyte-derived DCs to naturally circulating DC subsets. *Front Immunol* 5:165
  32. Dhodapkar MV, Steinman RM, Krasovsky J et al (2001) Antigen-specific inhibition of effector T cell function in humans after injection of immature dendritic cells. *J Exp Med* 193:233–238
  33. de Chickera SN, Snir J, Willert C et al (2011) Labelling dendritic cells with SPIO has implications for their subsequent in vivo migration as assessed with cellular MRI. *Contrast Media Mol I* 6:314–327
  34. Ahrens ET, Bulte JW (2013) Tracking immune cells in vivo using magnetic resonance imaging. *Nat Rev Immunol* 13:755–763
  35. Vuylsteke RJ, Molenkamp BG, Gietema HA et al (2004) Local administration of granulocyte/macrophage colony-stimulating factor increases the number and activation state of dendritic cells in the sentinel lymph node of early-stage melanoma. *Cancer Res* 64:8456–8460
  36. Takayama K, Yokozeki H, Ghoreishi M et al (1999) IL-4 inhibits the migration of human Langerhans cells through the downregulation of TNF receptor II expression. *J Invest Dermatol* 113:541–546
  37. Gonzales C, Yoshihara HA, Dilek N et al (2016) In vivo detection and tracking of T cells in various organs in a melanoma tumor model by <sup>19</sup>F-fluorine MRS/MRI. *PLoS One* 11:e0164557
  38. Castro O, Nesbitt AE, Lyles D (1984) Effect of a perfluorocarbon emulsion (Fluosol-DA) on reticuloendothelial system clearance function. *Am J Hematol* 16:15–21
  39. Dunn GP, Old LJ, Schreiber RD (2004) The immunobiology of cancer immunosurveillance and immunoeediting. *Immunity* 21:137–148
  40. Srinivas M, Turner MS, Janjic JM et al (2009) In vivo cytometry of antigen-specific T cells using <sup>19</sup>F MRI. *Magn Reson Med* 62:747–753
  41. Dashti A, Ebrahimi M, Hadjati J et al (2016) Dendritic cell based immunotherapy using tumor stem cells mediates potent antitumor immune responses. *Cancer Lett* 374:175–185
  42. Damo M, Wilson DS, Simeoni E, Hubbell JA (2015) TLR-3 stimulation improves anti-tumor immunity elicited by dendritic cell exosome-based vaccines in a murine model of melanoma. *Sci Rep* 5:17622
  43. Zhang Y, Liu X, Wang R et al (2018) Comparison of fusion protein and DC vaccine in inhibition of mouse B16F10 melanoma tumor. *Biomed Pharmacother* 97:784–792
  44. Jonuleit H, Kuhn U, Muller G et al (1997) Pro-inflammatory cytokines and prostaglandins induce maturation of potent immunostimulatory dendritic cells under fetal calf serum-free conditions. *Eur J Immunol* 27:3135–3142
  45. Melero I, Gaudernack G, Gerritsen W et al (2014) Therapeutic vaccines for cancer: an overview of clinical trials. *Nat Rev Clin Oncol* 11:509–524
  46. Farhood B, Najafi M, Mortezaee K (2019) CD8(+) cytotoxic T lymphocytes in cancer immunotherapy: A review. *J Cell Physiol* 234:8509–8521
  47. Steitz J, Bruck J, Steinbrink K et al (2000) Genetic immunization of mice with human tyrosinase-related protein 2: implications for the immunotherapy of melanoma. *Int J Cancer* 86:89–94
  48. Palazon A, Tyrakis PA, Macias D et al (2017) An HIF-1alpha/VEGF-A axis in cytotoxic T cells regulates tumor progression. *Cancer Cell* 32:669–683
  49. Boudewijns S, Bloemendaal M, Gerritsen WR et al (2016) Dendritic cell vaccination in melanoma patients: from promising results to future perspectives. *Hum Vacc Immunother* 12:2523–2528
  50. Hooijkaas AI, Gadiot J, van der Valk M et al (2012) Targeting BRAFV600E in an inducible murine model of melanoma. *Am J Pathol* 181:785–794
- Publisher's Note* Springer Nature remains neutral with regard to jurisdictional claims in published maps and institutional affiliations.